Decoherence-Induced Universality in Simple Metal Cluster Photoelectron Angular Distributions

Adam Piechaczek,[1] Christof Bartels,[1] Christian Hock,[1] Jan-Michael Rost,[2] and Bernd von Issendorff[1,*]
[1]Institute of Physics, University of Freiburg, Hermann-Herder-Straße 3, 79104 Freiburg, Germany
[2]Max-Planck-Institute for the Physics of Complex Systems, Nöthnitzer Straße 38, 01187 Dresden, Germany

(Received 13 January 2021; revised 26 March 2021; accepted 5 May 2021; published 11 June 2021)

Measured angular distributions of photoelectrons from size-selected copper and sodium cluster anions are demonstrated to exhibit a universal behavior independent of the initial electron state, cluster size, or material, which can be traced back to momentum conservation upon photoemission. Quantum simulations reproduce the universality under the assumption that multielectron dynamics localizes the emission on the cluster surface and renders the cluster opaque to photoelectrons, thereby quenching interference effects that would otherwise obscure this almost classical behavior.

DOI: 10.1103/PhysRevLett.126.233201

Employing Einstein's photoeffect, photoelectron spectroscopy is the key technique to study the electronic structure of matter. Yet photoemission is a highly complex process, an excitation of a system of many often strongly interacting electrons resulting in the emission of a single electron [1]. This multiparticle dynamics aspect constitutes a challenge for theory; predictions of energy or angular distributions of photoelectrons are often not completely satisfactory [2]. Experimental results for model systems could therefore help to improve the understanding and the treatment of such dynamics. Simple metal clusters like alkaline or noble metal clusters are very good candidates in this respect, as in the size range from a few up to several ten atoms they are clearly many-particle systems yet small enough to be treated by higher level methods. These clusters exhibit a highly discretized and well understood electron density of states, the so-called electron shell structure, consisting of angular momentum eigenstates slightly perturbed by the interaction with the nonspherical ion background [3–7]. We have shown previously that the angular distributions of photoelectrons emitted from such states in sodium cluster anions are strongly anisotropic, with a peculiar dependence on the photon energy (or more precisely the electron kinetic energy) that seems to depend mainly on the approximate angular momentum of the initial state of the electron [8]. The angular distributions strongly differ from what one would expect within effective single particle quantum models, which already gave hints at possible multiparticle dynamics involved in the photoemission process. Subsequent calculations performed by a number of groups [9–11] confirmed the important influence of multiparticle dynamics [9] but could not fully reproduce the experimental data.

We have now done additional measurements on copper cluster anions and will discuss them together with published and unpublished results for sodium cluster anions. It turns out that if presented as a function of a generalized final electron momentum, all angular distributions adopt a universal behavior independent of cluster size, cluster material, or the initial state of the electron. In order to understand and reproduce this universality, we employ a model that incorporates the decohering effect of multiparticle dynamics on an effective single-particle level. The decoherence quenches interferences and renders the photoelectron insensitive to the internal structure of the cluster, which together with the approximate angular momentum eigenstate character of the bound states gives rise to the observed universal behavior.

The experiments were performed with the same setup as described before [8] (see the Supplemental Material [12] for more details). Cluster anions were produced in a gas aggregation cluster source, thermalized in a cryogenic radio frequency ion trap, mass-selected in a reflectron time-of-flight mass spectrometer, and irradiated by pulses from a tunable laser in the interaction region of a velocity map imaging photoelectron spectrometer. The resulting electron images have been deconvoluted by a slightly modified p-Basex algorithm [20]. Measurements were repeated for a broad range of photon energies.

Copper clusters were chosen because copper, like sodium, is a monovalent s-p metal and can be seen as a free electron metal, although with stronger residual interactions. This is due to the presence of the fully occupied 3d band, 2–5.5 eV below the Fermi energy, that enhances the interatomic bonding via hybridization with the s-p band, thereby shortening the bonds and strongly increasing the free electron density. Furthermore, it strongly influences the dielectric response, leading to very different optical properties of copper [21] and sodium clusters [3]. A question therefore was how these additional interactions would influence the multielectron dynamics in general and the photoelectron angular distributions in particular.

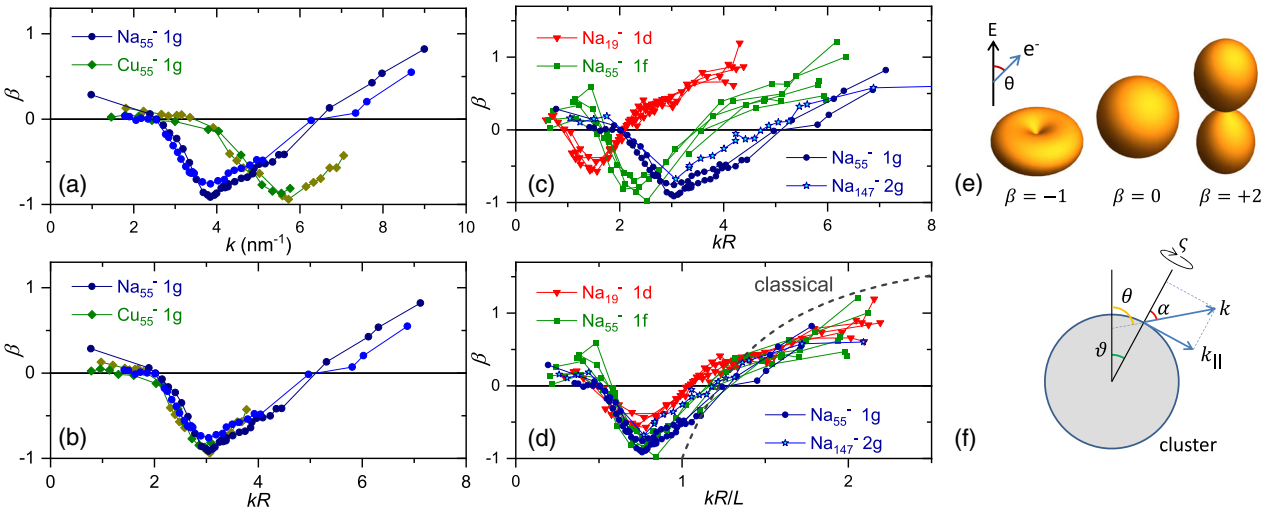

FIG. 1. (a) Anisotropy parameter of the angular distributions for the 1g-derived states of Na_{55}^- and Cu_{55}^- as a function of the final photoelectron momentum k (see Fig. S1 for the photoelectron spectra). (b) Same data as a function of the reduced momentum kR (R: cluster radius). (c) Anisotropy parameter as a function of kR for different states of different sodium cluster anions. (d) Same data as a function of kR/L, where L is the approximate angular momentum of the initial state of the electron. Gray dashed line: classical model. (e) Emission probability as a function of the angle θ between the emission direction and the electric field vector of the laser light for three values of the anisotropy parameter β. (f) Classical model: the electron is emitted from the cluster surface with an angle α to the surface normal, as determined by its momentum k and the surface projection $k_{||} = L/R$. The absorption probability depends on the angle ϑ, the emission angle θ on α, ϑ, and the azimuthal emission angle ζ (see text for details).

Results are shown in Fig. 1. As usual [22], the measured angular distributions are parameterized by the anisotropy parameter β as $I(\theta) = 1 + \beta(\frac{3}{2}\cos^2\theta - \frac{1}{2})$, where I is the electron intensity and θ is the angle between the emission direction and the light polarization [cf. Fig. 1(e)]. In Fig. 1(a), the dependencies of β on the photoelectron momentum k are shown for the two uppermost occupied states in Na_{55}^- and Cu_{55}^- clusters (photoelectron spectra of the clusters are shown in Fig. S1). As described earlier [5,23], both clusters possess an icosahedral structure. This is close to spherical but still causes the uppermost occupied angular momentum eigenstate, which in a spherical jellium model is a 1g state (with angular momentum quantum number $L = 4$ and radial quantum number 1) [3], to split up into two states of H_g and G_g character, respectively [5]. Despite their different binding energies these two states exhibit identical β curves, indicating that the overall wave function character of the underlying 1g state is preserved [8]. For both clusters, the curves exhibit a minimum where $\beta \sim -1$, which indicates photoelectron emission perpendicular to the laser polarization. This minimum occurs for different final momenta for the two clusters, which turns out to be due to their different radii. The angular distribution depends on transition matrix elements involving the wave functions of the bound and the continuum states; as the spatial extension of the wave functions of the bound states scales with the cluster radius, the wave functions of the continuum states have to be scaled accordingly. This can be achieved by plotting the β curve as a function of the dimensionless parameter kR, where R is the cluster radius (assuming a spherical cluster of bulk density). As one can see in Fig. 1(b), with this scaling the β curves of the 1g-derived states of the two clusters are close to identical. This is surprising in view of the differences of the electronic systems discussed above; it gives a hint that the photoelectrons are not sensitive to the internal structure of the cluster. The same scaling can be applied to angular distributions measured for different sodium cluster sizes, as demonstrated in Fig. 1(c). One can see that the scaled β curves of the 1g states of Na_{55}^- and the 2g states of Na_{147}^- coincide, which not only shows that the scaling works here as well but also that the radial motion of the electron within the cluster does not influence the angular distribution. One can furthermore notice that the minima of the curves shift roughly linearly with the angular momentum quantum number L of the initial electron state. Plotting the anisotropy parameter against a further reduced momentum kR/L therefore leads to the results in Fig. 1(d), where now all angular distributions practically coincide. This means that the angular distributions measured for different cluster sizes and materials can be traced back to a single universal function, which adopts small positive values of β for very small values of kR/L, approaches $\beta = -1$ for a value close to $kR/L = 1$, and exhibits a monotonous increase for larger kR/L.

The behavior of the curves in the region $kR/L > 1$ can be explained by a simple model. If one treats the cluster as a spherical box potential and uses the acceleration form of

the dipole operator, which is proportional to the gradient of the potential and therefore nonzero only at the cluster surface, photoemission can be interpreted to be localized at the surface. Furthermore, the electron momentum parallel to the surface will be approximately conserved; considering the surface as flat, in the long wavelength limit the combined effect of light and surface is translationally invariant parallel to the surface, which enforces the conservation of parallel momentum (a usual assumption for photoemission from surfaces [24]). For spherical box potentials, there is another important consequence: as the emission amplitude is proportional to the scalar product of the electric field vector and the gradient of the potential, for vertical light polarization the emission will be strongest on the upper and lower poles of the sphere and zero on its equator.

In a classical picture, the electron close to the surface has a momentum parallel to it of $k_{||} = L/R$. If the photon energy is chosen such that the emitted electron does not have any initial radial momentum, its final momentum k will be equal to $k_{||}$ and it will be emitted tangentially to the surface. As the emission happens mostly at the poles, the electron will therefore be emitted perpendicularly to the polarization, giving $\beta = -1$ for $k = L/R$. For larger values of the final momentum, the emission angle of the electron with respect to the surface normal will be $\alpha = \arcsin(k_{||}/k)$; probability weighted averaging over all emission locations on the cluster surface and the azimuthal angle in the plane parallel to the surface then yields [see Fig. 1(f) and Supplemental Material [12] for details]:

$$\beta = 2 - 3\left(\frac{L}{kR}\right)^2. \tag{1}$$

This curve is plotted in Fig. 1(d); indeed, it does have some resemblance to the scaled measured data. This already indicates that even in a real cluster the electrons might be seen as circulating within the cluster, with their parallel momentum conserved upon photoemission.

In a quantum treatment, one has to take into account that the dipole operator couples an initial state with angular momentum L to final states with angular momenta $L-1$ and $L+1$. In fact, the interference between these two emitted partial waves determines the angular distribution, so both their amplitudes and their relative phase shift matter. In simplified single electron models, initial and final wave functions can be readily calculated and can be used to determine radial transition dipole matrix elements and phase shifts. From these, with the help of the Cooper-Zare formula [25], which accounts for the averaging over initial states with different magnetic quantum numbers m_L, the anisotropy parameter of the angular distribution is obtained. Using the acceleration form of the dipole operator [26,27] and assuming a jellium-type potential with a sharp

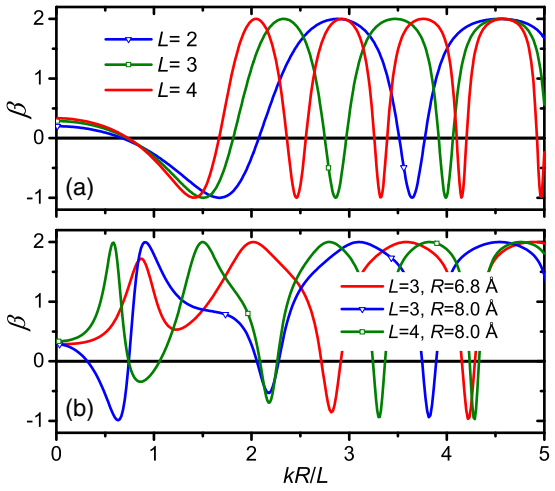

FIG. 2. (a) Anisotropy parameter as a function of the scaled final electron momentum kR/L for different initial angular momentum states of the electron, assuming vanishing photoelectron-cluster interaction. (b) Same as (a) but taking photoelectron-cluster interaction into account, by assuming a spherical box potential of 6 eV depth, for two initial angular momentum states and two cluster radii (of Na_{33}^- and Na_{55}^-).

edge (see Figs. S2 and S3 for a justification of this assumption), the radial transition matrix element reduces to the amplitude of the final state on the cluster surface [12]. The results are shown in Fig. 2 for two cases. In the first case, it is assumed that there is no interaction between the photoelectron and the cluster, a common simplification in the treatment of photoemission from anions [22]. Consequently the final states can be described by spherical Bessel functions, and the anisotropy parameters exhibit a rather simple behavior [Fig. 2(a)].

They do not reproduce the measurement, though. The value of $\beta = -1$ is obtained only for values of kR/L significantly larger than 1, which furthermore depend on L. For even larger values of kR/L, periodic oscillations of β can be seen, which are connected to Cooper minima [28] and within a semiclassical description can be traced back to destructive interference between electron trajectories launched from close to opposite points on the cluster surface [12]. If the interaction of the photoelectron with a finite depth spherical box potential is taken into account [12], β curves are obtained as shown in Fig. 2(b) for two cluster sizes and two angular momenta. One can observe a rather irregular behavior for small values of kR/L, which strongly depends on L and R (as well as the depth of the potential, which was kept constant here). The strong variations of β are due to so-called shape resonances [29], which are metastable states in the continuum bound by the centrifugal barrier. These lead to a strong energy dependence of the matrix elements and phase shifts. Previous calculations revealed similar resonances of the anisotropy parameter for sodium clusters [8,11,30]. For larger values of kR/L, again minima due to Cooper minima

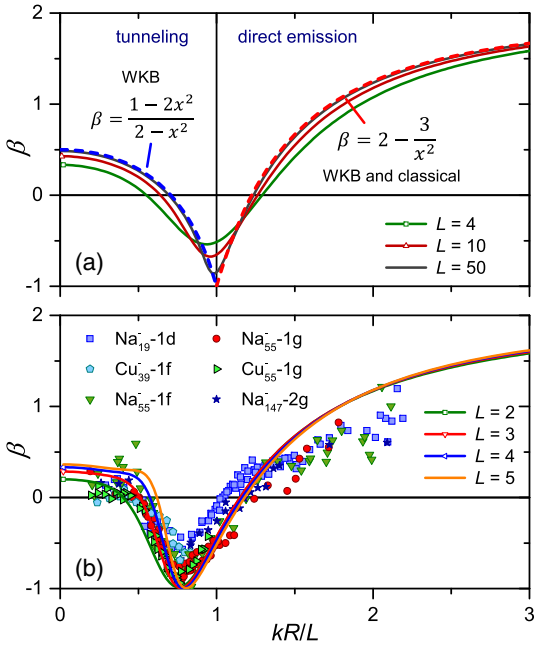

FIG. 3. (a) Comparison of three model calculations of angular distributions (electron-cluster interaction neglected): classical calculation, assuming outward electron emission with conservation of tangential momentum (dashed red line); WKB-like treatment of the photoemission, assuming complete opaqueness of the cluster for the photoelectrons (dashed red and blue line), giving results identical to the classical ones in the direct emission regime; quantum calculation for different initial angular momentum states assuming free electron continuum waves subject to an absorptive boundary condition at the cluster surface (green, dark red, and dark gray line). The results converge to the classical and semiclassical ones for large L. (b) Similar calculation, additionally taking the exchange-correlation interaction between the emitted electron and the cluster into account [12], for Na_{55}^- and four initial angular momenta in comparison to the data from Fig. 1(d) and copper cluster results (see Fig. S5 for further examples).

can be seen. In contrast the measurements exhibit a much simpler behavior, without any hint at interference induced oscillations or shape resonances—apparently these coherent effects are quenched. An explanation can be obtained from measurements of electron attachment cross sections for gas phase neutral sodium clusters [31]. Here, it was shown that, for low electron energies, the cross sections strongly increase due to the image charge interaction of the electron with the cluster, which bends the electron trajectory toward the cluster. Such an increase of the attachment cross section can only result if the electron does not traverse the cluster but is stopped in it; the cluster therefore must be rather opaque for low energy electrons. This opaqueness will have a strong effect on the photoemission, as it should suppress interferences between photoelectron trajectories in case one of the trajectories passes through the cluster. Furthermore, it will quench metastable states and therefore suppress resonance effects. In order to take this electron absorption by the cluster into account, in the calculations an exponential decay of the final wave function within the cluster was assumed [12] (see Fig. S4 for an illustration); resulting anisotropy parameters are shown in Fig. 3(a). Both the effects of shape resonances and Cooper minima have vanished; furthermore, the results are now almost independent of the initial angular momentum L. For larger L, the curves converge to the classical result discussed above. In fact, for very large L, one can simplify the treatment and use a WKB-like [32] approach to calculate matrix elements and phase shifts [12]. This exactly reproduces the classical results for $kR/L > 1$ and also provides an analytical large L limit for $kR/L < 1$, where the electrons have to tunnel through the centrifugal barrier.

Even better agreement with experiment is obtained if the image charge potential or more precisely the exchange-correlation potential (Fig. S2) is taken into account, again in line with the findings of Kasperovich *et al.* [31]. In this case, one has to integrate the Schrödinger equation numerically [12]. Resulting anisotropy parameters are shown in Fig. 3(b); they reproduce the general features of the experimental result very well. The universal form of the angular distributions can now be fully explained: upon photoemission the electron retains its momentum parallel to the surface, which would lead to an emission perpendicular to the light polarization in the case of zero radial momentum and absent final interaction with the cluster. The exchange-correlation interaction both bends the electron trajectory and slows down the electron. As a consequence, perpendicular emission occurs for electrons that initially have some outward radial momentum but are asymptotically slowed down to values slightly below kR/L. For very small values of kR/L, tunneling through the centrifugal barrier suppresses the contribution of the partial wave with angular momentum $L+1$, resulting in a small positive value of β. For values of kR/L larger than 1, the electron emission gets more and more perpendicular to the cluster surface and therefore parallel to the light polarization. Since the cluster is opaque, there is no interference of trajectories from opposite parts of the cluster that would lead to strong variations of the partial wave amplitudes and therefore also of β—consequently, there is a monotonic convergence toward parallel emission. Note that the universal function describes the angular distributions well for $L \geq 2$. For s states, there is no prediction as kR/L diverges; for p states the measured curves exhibit a weaker minimum than predicted (see Fig. S5), which might be due to additional damping effects affecting these very low energy photoelectrons.

These results deserve some remarks. It is surprising that close to identical angular distributions are obtained for different cluster sizes with different geometric structures and especially for different cluster materials. But the point is that the photoemission happens at the cluster surface

and that only outgoing electrons make it into the continuum, due to which the emission is practically insensitive to the internal electronic or geometric structure of the cluster. All that is needed is that the emitted electron has a sufficiently well-defined initial angular momentum. Nevertheless, this simple behavior is a result of complex dynamics. The fact that the electron occupies a state close to an angular momentum eigenstate and is emitted from the cluster surface is due to the spherical boxlike effective single-particle potential of the cluster, which itself is the result of the interaction of all electrons. The opaqueness of the cluster is a consequence of the many low-lying excited states of the electronic system; similarly the long range exchange-correlation interaction requires a concerted dynamics of all electrons. Thus it is intricate many-electron dynamics which leads to this almost classical single-particle behavior of the emitted electron. Similar results are expected for emission processes from other simple Fermi systems with spherical or cylindrical symmetry such as electron emission from metal nanowires or atom emission from spherical clouds of cold fermionic atoms in a trap. This simple and very distinct phenomenon constitutes a benchmark challenge for multiparticle quantum theory and thereby could help to improve our general understanding of small Fermi-system dynamics.

This work has been supported by the Deutsche Forschungsgemeinschaft.

*Corresponding author.
bernd.von.issendorff@uni-freiburg.de

[1] L. S. Cederbaum, W. Domcke, J. Schirmer, and W. von Niessen, Adv. Chem. Phys. **65**, 115 (1986).
[2] C. M. Oana and A. I. Krylov, J. Chem. Phys. **131**, 124114 (2009).
[3] W. A. de Heer, Rev. Mod. Phys. **65**, 611 (1993).
[4] G. Wrigge, M. Astruc Hoffmann, and B. v. Issendorff, Phys. Rev. A **65**, 063201 (2002).
[5] H. Häkkinen, M. Moseler, O. Kostko, N. Morgner, M. Astruc Hoffmann, and B. v. Issendorff, Phys. Rev. Lett. **93**, 093401 (2004).
[6] C.-Y. Cha, G. Ganteför, and W. Eberhardt, J. Chem. Phys. **99**, 6308 (1993).
[7] J. Eaton, L. Kidder, H. Sarkas, K. McHugh, and K. Bowen, in *Physics and Chemistry of Finite Systems: From Clusters to Crystals*, NATO Science Series C, edited by P. Jena *et al.* (Kluwer Academic, Dordrecht/Boston, 1992), Vol. 374, p. 493.
[8] C. Bartels, C. Hock, J. Huwer, R. Kuhnen, J. Schwöbel, and B. v. Issendorff, Science **323**, 1323 (2009).
[9] R. G. Polozkov, V. K. Ivanov, A. V. Korol, and A. V. Solov'yov, Eur. Phys. J. D **66**, 287 (2012).
[10] P. Wopperer, P.-G. Reinhard, and E. Suraud, Ann. Phys. **525**, 309 (2013).
[11] K. Jänkälä, Eur. Phys. J. D **67**, 65 (2013).
[12] See Supplemental Material, which includes Refs. [13–19], at http://link.aps.org/supplemental/10.1103/PhysRevLett.126.233201 for additional figures, methods, and theoretical derivations.
[13] C. Bartels, C. Hock, R. Kuhnen, and B. v. Issendorff, J. Phys. Chem. A **118**, 8270 (2014).
[14] A. T. J. B. Eppink and D. H. Parker, Rev. Sci. Instrum. **68**, 3477 (1997).
[15] W. Ekardt, Phys. Rev. B **29**, 1558 (1984).
[16] P.-A. Hervieux, M. E. Madjet, and H. Benali, Phys. Rev. A **65**, 023202 (2002).
[17] P. Rinke, K. Delaney, P. García-González, and R. W. Godby, Phys. Rev. A **70**, 063201 (2004).
[18] G. Bertsch, Comput. Phys. Commun. **60**, 247 (1990).
[19] H.-P. Cheng, R. S. Berry, and R. L. Whetten, Phys. Rev. B **43**, 10647 (1991).
[20] G. A. Garcia, L. Nahon, and I. Powis, Rev. Sci. Instrum. **75**, 4989 (2004).
[21] S. Lecoultre, A. Rydlo, C. Felix, J. Buttet, S. Gilb, and W. Harbich, J. Chem. Phys. **134**, 074303 (2011).
[22] A. Sanov, Annu. Rev. Phys. Chem. **65**, 341 (2014).
[23] O. Kostko, B. Huber, M. Moseler, and B. von Issendorff, Phys. Rev. Lett. **98**, 043401 (2007).
[24] S. Hüfner, *Photoelectron Spectroscopy: Principles and Applications*, 3rd ed., Advanced Texts in Physics (Springer-Verlag, Berlin Heidelberg, 2003).
[25] J. Cooper and R. N. Zare, J. Chem. Phys. **48**, 942 (1968).
[26] H. A. Bethe and E. E. Salpeter, *Quantum Mechanics of One- and Two-Electron Atoms* (Springer-Verlag, Berlin Heidelberg, 1957).
[27] O. Frank and J. M. Rost, Z. Phys. D **38**, 59 (1996).
[28] J. W. Cooper, Phys. Rev. **128**, 681 (1962).
[29] G. J. Schulz, Rev. Mod. Phys. **45**, 378 (1973).
[30] A. V. Solov'yov, R. G. Polozkov, and V. K. Ivanov, Phys. Rev. A **81**, 021202(R) (2010).
[31] V. Kasperovich, K. Wong, G. Tikhonov, and V. V. Kresin, Phys. Rev. Lett. **85**, 2729 (2000).
[32] M. V. Berry and K. E. Mount, Rep. Prog. Phys. **35**, 315 (1972).